










ARTICLE

Comparative assessment of satellite- and drone-based vegetation indices to predict arthropod biomass in shrub-steppes

J. Traba^{1,2}  | J. Gómez-Catasús^{1,2,3}  | A. Barrero^{1,2}  |
D. Bustillo-de la Rosa^{1,2}  | J. Zurdo^{1,2}  | I. Hervás^{1,2} | C. Pérez-Granados^{1,4}  |
E. L. García de la Morena^{1,5}  | A. Santamaría^{1,2}  | M. Reverter^{1,2} 

¹Terrestrial Ecology Group (TEG-UAM).
Department of Ecology, Universidad
Autónoma de Madrid, Madrid, Spain

²Centro de Investigación en Biodiversidad
y Cambio Global, Universidad Autónoma
de Madrid, Madrid, Spain

³Novia University of Applied Sciences,
Ekenäs, Finland

⁴Ecology Department, Alicante
University, Alicante, Spain

⁵Biodiversity Node S.L. Sector Foresta,
Madrid, Spain

Correspondence

J. Gómez-Catasús

Email: julia.gomez@uam.es

Funding information

BBVA Foundation, BBVA Dron Ricoti
project; European Commission, Grant/
Award Number: LIFE15-NAT-ES-000802;
REMEDINAL-3 from CAM; European
Commission, Grant/Award Number:
LIFE20-NAT-ES-000133

Handling Editor: Juan C. Corley

Abstract

Arthropod biomass is a key element in ecosystem functionality and a basic food item for many species. It must be estimated through traditional costly field sampling, normally at just a few sampling points. Arthropod biomass and plant productivity should be narrowly related because a large majority of arthropods are herbivorous, and others depend on these. Quantifying plant productivity with satellite or aerial vehicle imagery is an easy and fast procedure already tested and implemented in agriculture and field ecology. However, the capability of satellite or aerial vehicle imagery for quantifying arthropod biomass and its relationship with plant productivity has been scarcely addressed. Here, we used unmanned aerial vehicle (UAV) and satellite Sentinel-2 (S2) imagery to establish a relationship between plant productivity and arthropod biomass estimated through ground-truth field sampling in shrub steppes. We UAV-sampled seven plots of 47.6–72.3 ha at a 4-cm pixel resolution, subsequently downscaling spatial resolution to 50 cm resolution. In parallel, we used S2 imagery from the same and other dates and locations at 10-m spatial resolution. We related several vegetation indices (VIs) with arthropod biomass (epigeous, coprophagous, and four functional consumer groups: predatory, detritivore, phytophagous, and diverse) estimated at 41–48 sampling stations for UAV flying plots and in 67–79 sampling stations for S2. VIs derived from UAV were consistently and positively related to all arthropod biomass groups. Three out of seven and six out of seven S2-derived VIs were positively related to epigeous and coprophagous arthropod biomass, respectively. The blue normalized difference VI (BNDVI) and enhanced normalized difference VI (ENDVI) showed consistent and positive relationships with arthropod biomass, regardless of the arthropod group or spatial resolution.

J. Traba and J. Gómez-Catasús contributed equally to this study.

This is an open access article under the terms of the [Creative Commons Attribution-NonCommercial-NoDerivs](https://creativecommons.org/licenses/by-nc-nd/4.0/) License, which permits use and distribution in any medium, provided the original work is properly cited, the use is non-commercial and no modifications or adaptations are made.

© 2022 The Authors. *Ecological Applications* published by Wiley Periodicals LLC on behalf of The Ecological Society of America.

Our results showed that UAV and S2-VI imagery data may be viable and cost-efficient alternatives for quantifying arthropod biomass at large scales in shrub steppes. The relationship between VI and arthropod biomass is probably habitat-dependent, so future research should address this relationship and include several habitats to validate VIs as proxies of arthropod biomass.

KEYWORDS

arthropod biomass, coprophagous arthropods, epigeous arthropods, shrub steppe, vegetation index

INTRODUCTION

Arthropods play a fundamental role in ecosystem functions, such as pollination, pest control, and organic decomposition (Losey & Vaughan, 2006), and are a key food item for many species (Báldi & Kisbenedek, 1997; Weiss et al., 2013). Arthropod biomass and diversity are usually associated with plant productivity, as decreases in quantity of forage seem to reduce the amount of plant consumers (the more-individuals hypothesis; Kaspari et al., 2003; Srivastava & Lawton, 1998). Moreover, plant health relates to nutrient availability, which may directly affect plant biomass and indirectly arthropod communities (Haddad et al., 2001; Siemann, 1998). In summary, plant biomass and quality, as well as specific vegetation structure or composition, are related to arthropod biomass both for the whole community (Dennis et al., 1998; Harrison et al., 2018; Prather & Kaspari, 2019) and for distinct taxonomic or functional groups (Báldi & Kisbenedek, 1997; Labadessa et al., 2015; Smith et al., 2020; Weyer et al., 2012). Despite these considerations, establishing general relationships of arthropod biomass with specific plant characteristics may be tricky, especially at large spatial scales, owing to the great diversity of the arthropod group in its size, mobility, trophic level, life history, and microhabitat preferences, including plant structure and composition (Southwood et al., 1979). Therefore, a more general evaluation of its relationship with plant productivity remains a challenge (but see Sweet et al., 2015 and Fernández-Tizón et al., 2020).

Remote sensing has the capacity to map and quantify plant productivity in different types of natural and anthropogenic influenced plant communities and land uses (Díaz-Delgado et al., 2017). For several decades, various satellite platforms, as MODIS, Landsat, and other mid-spatial-resolution (tens of meters) satellites have been used to explore and map plant productivity and other vegetation characteristics at large scales (e.g., Möller et al., 2017). Recently, Sentinel-2 (S2) has emerged as a major asset (Belgiu & Csillik, 2018; Inglada et al., 2015), basically for its

medium spatial (10 m), high radiometric (13 spectral bands), and rapid temporal (revisit time of 5 days at the equator) resolutions, together with its free cost. Theoretically, it would be relatively easy to test for relationships between satellite-extracted plant productivity and other biologically relevant variables different than—but related to—plant productivity. This could be the case with animal biomass, for example, when a relation between plants and animals is predicted. However, the spatial resolution of free satellite imagery could be too coarse to establish accurate relationships at fine scales, such as that between plant productivity and arthropod biomass. The use of unmanned aerial vehicles (UAVs), which work on high- and very high-resolution imagery and make it possible to obtain multiple images of different dates at relatively low cost, may help to test these relationships. UAVs have been used to provide reliable estimates of plant biomass, productivity, and greenness (Colomina & Molina, 2014; Pla et al., 2019; Strong et al., 2017) and even to differentiate among species (Salamí et al., 2014), but on a few occasions these relationships have been tested at larger spatial scales, where UAV use may be inefficient (Fraser et al., 2017; Pla et al., 2019). In short, the combination in UAVs of multispectral sensors and photogrammetric-derived information allows for map productivity at very detailed scales and makes it possible to detect short-term changes and thus provide rapid assessment for the management and conservation of other organisms, such as mammals (Vermeulen et al., 2013) or breeding bird colonies (Sardà-Palomera et al., 2012). On the other hand, fine- and medium-resolution remote sensing has the potential to allow extrapolations to remote and nonsampled areas, but to our knowledge it has been scarcely used to relate other key elements in ecosystems, such as arthropod biomass.

Among the remote sensing-derived products more often used are plant productivity or greenness indicators, frequently named vegetation indices (VIs). VIs are mathematical combinations based on digital values of spectral bands, in a way designed to produce a simple value that indicates the amount or plant vigor (greenness,

productivity) of vegetation within a pixel, estimated as a function of the radiation that plants emit or reflect (Rouse et al., 1974). VIs can be used for detecting changes in photosynthetic activity and plant spatial heterogeneity in order to evaluate for phenology, plant stress situations, damage or conditions, and differences in soil moisture, for example, which in turn can be used to explain other ecological relationships (Colomina & Molina, 2014; Huete et al., 1997; Imran et al., 2020; Inglada et al., 2015). VIs are related to the proportion of radiation absorbed by photosynthetic tissues and are linearly correlated with vegetation features like the leaf area index (LAI) and plant biomass (Hunt et al., 2010; Kross et al., 2015; Prabhakara et al., 2015). Thus, VIs can capture complex ecological information about canopy structure, aboveground biomass and leaf traits, or proportion of photosynthetic and nonphotosynthetic parts, such as leaf dry matter and bare ground (Ollinger, 2011; Serrano et al., 2000).

The normalized difference VI (NDVI) (Rouse et al., 1974) is the VI most often used (see a review in Pettorelli et al., 2011). The majority of VIs are an adaptation from NDVI and are calculated by combining two or more spectral bands. For instance, using the green band instead of the red band allows the VI to be less sensitive to variations in ground cover as vegetation has a higher level of reflectance for green wavelengths (Gitelson et al., 1996; Sripada et al., 2006). The blue channel, as in the blue NDVI (BNDVI), amplifies chlorophyll absorption by summing both near-infrared (NIR) reflectance and green channel reflectance, and have proved useful for vegetation monitoring and a better parameterization of plant health indicators (Rasmussen et al., 2016). These other VIs may operate better under determined circumstances and reduce negative effects attributed to NDVI, such as those related to atmospheric conditions and soil background (Huete et al., 1997). In addition, VIs using blue or green channels may perform well when trying to relate them to biological parameters (Gitelson et al., 1996; Strong et al., 2017).

Finding simple and low-cost methods to quantify arthropod abundance or biomass is an important objective in ecology because it would provide sensitive data for many uses, including conservation, while improving the high cost–benefit ratio of field sampling. Field sampling of plant structure (plant height and cover, frequently by species) and arthropods (e.g., pitfall traps, sweep net sampling) is very time consuming and expensive and usually provides information on just a few located points. In contrast, UAV and satellite platforms provide affordable or even free medium- to high-resolution imagery, offering repeatability in time and space, and can be used in remote areas (Colomina & Molina, 2014; Strong et al., 2017). These characteristics make it a potential cost-efficient tool for estimating arthropod biomass.

In this study we aimed to test for relationships between plant biomass (estimated through different VIs) and arthropod biomass (epigeous, coprophagous, and consumer groups: predatory, detritivore, phytophagous, and diverse) when working at fine (UAV) and medium (S2) spatial resolution, under the hypothesis of a positive relationship between these two ecosystem components and that this relationship can be detected at both small and large spatial scales. Owing to the assumed strong site-specific habitat-dependent relationships between arthropods and plant productivity (Weiss et al., 2013) and its remote sensing-derived information, we tested them in a single ecosystem, the natural Iberian shrub-steppe habitats (“paramos”) in Central Spain. Natural steppe habitats are one of the most rare and threatened habitats in Europe (Sainz Ollero, 2013). In Spain, the Iberian “paramos” represent an important habitat of Iberian steppes (Sainz Ollero, 2013) and hold singular communities of plants, arthropods, and birds (Traba et al., 2013; Zurdo et al., 2021), which are intimately interrelated. Several studies detected significant relationships between plant structure, arthropod availability, and threatened insectivorous bird species in these Iberian “paramos,” which point to a complex system of multiple interactions where plant structure and composition modulates arthropod biomass and composition, which in turn affects the abundance and space use of insectivorous birds (Gómez-Catasús et al., 2019; Reverter et al., 2019; Smith et al., 2020). As a consequence, some steppe bird species of high conservation interest have their strongholds in these Iberian “paramos” (Traba et al., 2013), such as the Dupont’s lark (*Chersophilus duponti*), the greater short-toed lark (*Calandrella brachydactyla*), and the tawny pipit (*Anthus campestris*), which makes it of even greater interest to investigate the relationship between plants and arthropods. Besides the relative homogeneous landscape and simple vegetation structure of these shrub-steppe habitats (dominated by small height scrublands and grasslands), bird distribution is not homogeneous and seems to respond to spatial heterogeneity at a fine scale in plant and arthropod availability (Gómez-Catasús et al., 2019; Reverter et al., 2019, 2021), so high- and medium-resolution remote sensing can help us to better understand these complex ecological relationships at an appropriate scale.

METHODS

Study area

The study area is located in the Iberian System (Soria, central Spain) (Figure 1a), within the Altos de Barahona and Páramo de Layna Special Areas of Conservation (SAC) and Special Protection Areas (SPAs) of the

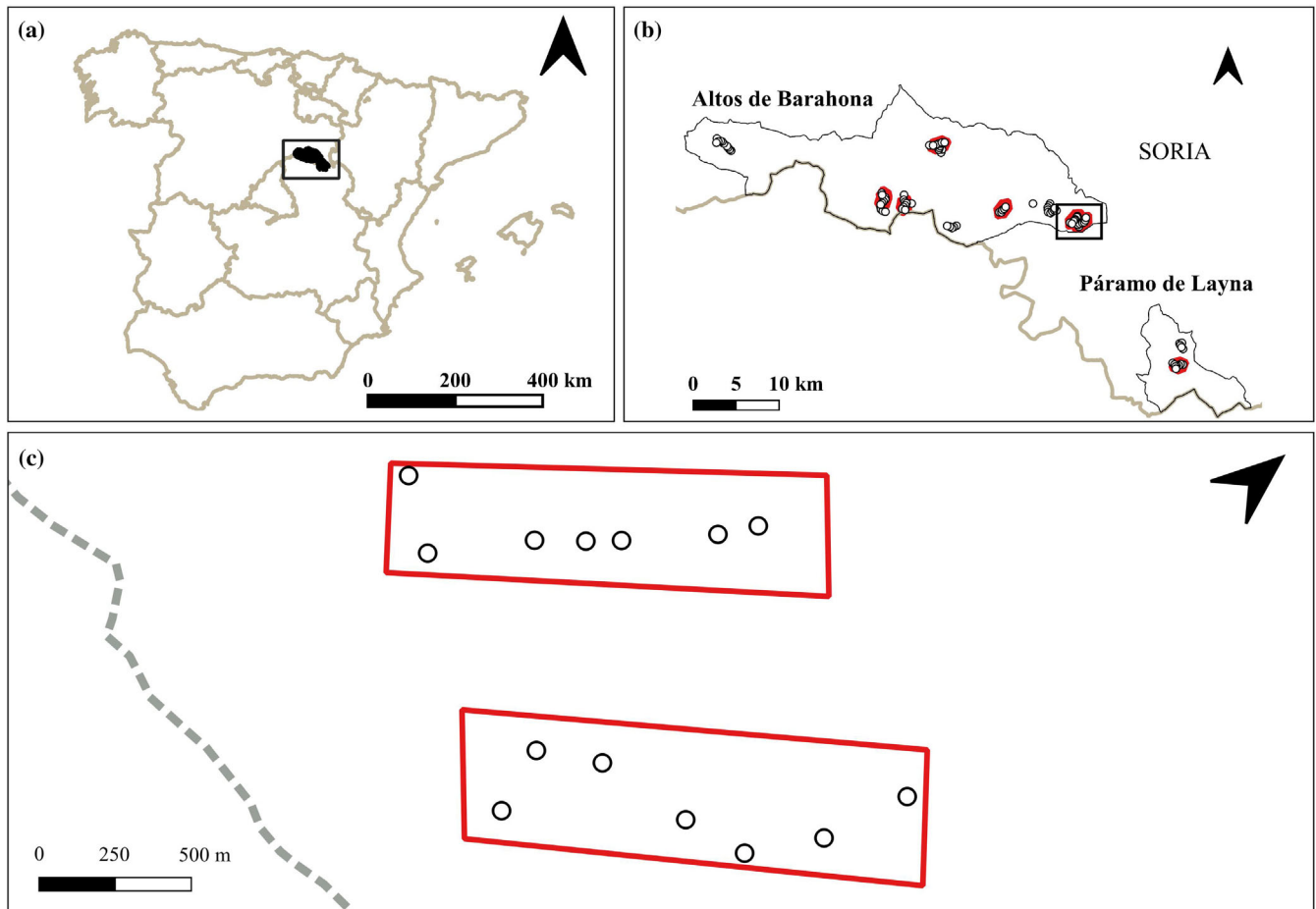


FIGURE 1 (a) Location of study area in Soria province, central Spain (black rectangle). (b) Zoom to study area in southern Soria. Sampling stations (white dots) and unmanned aerial vehicle (UAV) plots (red limits) are depicted. The name of the Special Areas of Conservation (SAC) and Special Protection Areas (SPA) for birds of European Union's Natura 2000 Network (ES4170148 and ES4170120, respectively) are indicated in bold, along with their limits indicated (black line). (c) Zoom to two UAV plots (black rectangle in panel b), with UAV plots (red areas) and sampling stations (white dots). The limits of Altos de Barahona SPA (dashed gray line).

European Union's Natura 2000 Network (ES4170148 and ES4170120, respectively; Figure 1b). They are located in the 10×10 Universal Transverse Mercator (UTM) zones 30TWL16, 17, 26, 27, 36, 37, 46, and 55. The whole study area covers around 50,400 ha in both SACs. The relief is gentle or plain (excluding river canyons, not considered in this study), located around 1100–1200 m above sea level. Soils are shallow with rocky substrate. Climate is continental Mediterranean, with a mean temperature of 10.8°C and a mean annual rainfall of 471 mm (Aranbarri et al., 2015).

These areas are of conservation interest owing to the steppe bird community they hold, particularly Dupont's lark, and include several European habitats of interest (Zurdo et al., 2021). The plant communities are dominated by continental scrublands and mixed grassland–scrublands, such as *Genista pumila*, *G. scorpius*, *Thymus* spp., *Satureja intricata*, dry perennial grasslands, and xerophytic grasslands on carbonate substrates (Sainz Ollero & van

Staalduinen, 2012; Zurdo et al., 2021). Crops, plowed fields, and pine afforestations are interspersed in the area, though they were explicitly excluded from the study.

Field sampling—Arthropod biomass

We located a total of 92 field-sampling stations to estimate arthropod biomass, but not all were placed in all sampling years: 79 in 2017 and 67 in 2018 and 2019 (Table 1). Sampling stations were separated by a mean distance of 271.7 m (SD = 170.9; minimum and maximum distances to the nearest sampling station were 117.1 and 1781.3 m, respectively). Arthropod biomass was sampled once in winter (January/February), summer (July), and autumn (September/October), and three times during spring (April, May, and June) in 2017, 2018, and 2019 (Table 1). Sampling stations were not placed in winter 2018 due to unfavorable weather conditions.

TABLE 1 Number of sampling stations located per month and year in whole study area (sampling stations) and within unmanned aerial vehicle (UAV) flight plots (sampling station UAV plots).

Season	Month	Sampling stations	Sentinel-2 imagery	Sampling stations UAV plots	UAV flights
2017					
Spring	April	79	Yes	0	No
	June	79	Yes	41	Yes (6)
Summer	July	79	Yes	0	No
Autumn	October	79	Yes	41	Yes (6)
2018					
Spring	April	67	No	48	Yes (7)
	June	67	Yes	48	Yes (7)
Summer	July	67	Yes	0	No
Autumn	October	67	Yes	48	Yes (7)
2019					
Winter	January	67	Yes	0	No
Spring	May	67	Yes	0	No
	June	67	Yes	0	No
Summer	July	67	Yes	0	No
Autumn	September	67	Yes	0	No

Note: We indicate whether Sentinel-2 and UAV imagery were available for each sampling period. Lastly, we indicate within brackets the number of plots where the UAV flights were carried out. Those samplings for which neither Sentinel-2 nor UAV imagery was available are omitted.

Terrestrial ground-dwelling arthropods were sampled using three pitfall traps per sampling station, placed at 5-m intervals. Pitfall traps consisted of a plastic cup of 230 ml, 7 cm in diameter and 10 cm in depth, with holes at the top to ease rain drainage. Plastic cups were buried and protected by a PVC tube to prevent its collapse and filled with 175 ml 40% ethylene glycol and a drop of soap to reduce surface tension. Traps were active for 7 days then filtered, and animals were stored in 70% ethanol. Although flying arthropods also fell into the pitfall traps, we carried out a specific sampling of flying arthropods at the moment the pitfall traps were collected in order to cover all taxa. For that, we walked two 10-m transects per sampling station with an entomological sweep net. The trapped individuals were stored in the same bottle as ground-dwelling arthropods, and they were considered together, hereafter referred to as epigeous arthropods. For more details about the sampling methodology, see Reverter et al. (2021) or Gómez-Catasús et al. (2019).

Coprophagous arthropods were sampled at each sampling station, with one baited pitfall trap, consisting of a 20-cm-diameter plastic container baited with 200 g fresh local sheep dung. Traps were active for 1 day, just after the collection of epigeous pitfall traps and under similar weather conditions in all sampling stations. Coprophagous

arthropods were stored in 70% ethanol, and only those individuals with coprophagous habits were identified: order *Coleoptera* family *Scarabaeidae* (*Gymnopleurus* spp., *Onthophagus* spp., and *Scarabeus* spp.) and order *Diptera* suborder *Brachycera*.

We determined arthropods at least to taxonomic order. We estimated arthropod biomass using the specific equations from Hódar (1996):

$$W = \alpha \times BL^b$$

where *W* is biomass in milligrams, *BL* is body length (in millimeters), and α and *b* are specific parameters for each group (or each order) (Hódar, 1996). We measured body length (excluding legs, antennae, and other appendices) in a maximum of 15 individuals per sample, using a digital caliper (± 0.01 mm). To minimize observer bias, all samples were identified by the same researcher (MR). For a similar methodology for estimation of invertebrate biomass see Traba et al. (2007), Gómez-Catasús et al. (2019), or Reverter et al. (2021). Lastly, we classified epigeous arthropod taxa into consumer groups (predatory, detritivore, phytophagous, and diverse; Appendix S1) and calculated the biomass per arthropod consumer group.

Since three pitfall traps were placed per sampling station, the biomass of epigeous arthropods (terrestrial + flying) per station and sampling period was estimated as the mean biomass of the pitfall traps that were active after 7 days. Lastly, coprophagous arthropod biomass was estimated as the total biomass measured in each sampling station, since only one baited pitfall trap was placed per sampling station. If a trap was invalidated, it was noted as missing data.

UAV imagery collection

We selected seven plots ranging from 47.6 to 72.3 ha (mean \pm SD = 60.0 \pm 9.6) within the general study area (Figure 1b). Plots were similar in relation to altitude, relief, slope, and plant communities. A total of 41 sampling stations were placed within six plots in 2017 and 48 sampling stations within seven plots in 2018 out of the aforementioned 92 sampling stations (Table 1).

At five time points during 2017 and 2018, we carried out up to 65 flights, with close to 28 flight hours and 1290 km traveled, with a total of 20,881 images obtained. A summary of the flights can be found in Appendix S2. Specific flight dates were always close to the field sampling addressed to estimate arthropod biomass (see preceding information; Table 1).

High-resolution UAV images were collected using a fixed-wing drone (SRPAS model A2) flying 120 m above the ground (equivalent to a focal length of 5.2 mm), which offered a resolution on the ground (ground sampling distance) of 4 cm/pixel. In general, each of the seven study plots was completely covered in a single flight, although some minor sections or even the entire sector was repeated in case of technical or meteorological incidents.

The sensor was a Canon S100 camera modified to capture the red edge (RE) spectrum (~770 nm; filter Event38), with a 1/1.7 in. (0.75 \times 0.56 cm) CMOS sensor and 12 MP resolution. This modified sensor provides images along three discrete spectral bands: RE, green, and blue. Despite the relatively low-accuracy band-discrimination capacity of such modified cameras compared to those of traditional multispectral cameras, they offer good solutions with a high cost–benefit relationship for estimating productivity indices in agriculture or field ecology (Lebourgeois et al., 2008; Salamí et al., 2014). The RE channel was around 770 nm, which may correspond to a midposition between Channels 6 and 7 in S2. Image postprocessing consisted in (i) georeferencing (in the WGS84 system) and altitude registering; (ii) image aligning and building of a digital elevation model (DEM) and orthomosaic using the Agisoft Metashape Professional photogrammetry software (version 1.4). Georeferencing

was done with four to six permanent ground control points per study plot, determined with submeter precision using a global navigation satellite system with differential correction in real time, Emlid Reach. Finally, (iii) we down-scaled the resolution of the orthophotos to 50 cm/pixel while calculating the different VIs, in order to reduce the size of the files and facilitate data processing but maintaining a high spatial resolution.

Sentinel-2 imagery collection

We used free S2 imagery atmospherically corrected, corresponding to the 30TVL and 30TWL zones, where all 92 field-sampling points were located (see subsequent discussion). We selected available cloud-free images corresponding to the closest date to each arthropod field sampling (Table 1), always on the same date for both UTM zones. Imagery was obtained from the LandViewer page (eos.com). We used blue, green, red, and NIR (Channel 8) bands to calculate the VIs, at a spatial resolution of 10 m.

Vegetation indices

We calculated the following VIs for UAV imagery and the same indices and NDVI for S2 imagery: BNDVI, enhanced NDVI (ENDVI), green infrared percentage VI (GIPVI), green NDVI (GNDVI), green ratio VI (GRVI), green soil adjusted VI (GSAVI), (see Table 2). All these indices were obtained by applying the corresponding formula (Table 2) on the digital numbers coming from the corresponding channels of the UAV or S2 imagery and saved in a raster layer with a Tagged Image File (TIF) extension. VIs from the UAV imagery were calculated using the RE band instead of the NIR band because the modified sensor employed did not provide images along the NIR spectral band (see the *UAV imagery collection* section). Previous studies demonstrated that VIs calculated using RE and visible bands showed similar performance in estimating variables associated with plant productivity, vigor, and health than those using NIR (Imran et al., 2020; Upadhyay et al., 2013). In our case, S2-derived VIs calculated using both RE and NIR bands were highly correlated, leading to similar results (Appendix S3).

We calculated VIs assigned to each arthropod sampling station as the average of each index in a 50-m buffer around the central point of each sampling station, for both UAV and S2 imagery. VI calculations, zone statistics, and spatial joining were carried out in an open geographic information system (GIS) (Quantum GIS Development Team, 2020).

TABLE 2 Formulas used to calculate each vegetation index.

Index	Description	Formula	Reference
NDVI	Normalized difference vegetation index	$\frac{\rho_{NIR} - \rho_{Red}}{\rho_{NIR} + \rho_{Red}}$	
BNDVI	Blue normalized difference vegetation index	$\frac{\rho_{NIR} - \rho_{Blue}}{\rho_{NIR} + \rho_{Blue}}$	
ENDVI	Enhanced normalized difference vegetation index	$\frac{(\rho_{NIR} + \rho_{Green}) - (2 \times \rho_{Blue})}{(\rho_{NIR} + \rho_{Green}) + (2 \times \rho_{Blue})}$	
GIPVI	Green infrared percentage vegetation index	$\frac{\rho_{NIR}}{\rho_{NIR} + \rho_{Green}}$	Crippen (1990)
GNDVI	Green normalized difference vegetation index	$\frac{\rho_{NIR} - \rho_{Green}}{\rho_{NIR} + \rho_{Green}}$	Gitelson et al. (1996)
GRVI	Green ratio vegetation index	$\frac{\rho_{NIR}}{\rho_{Green}}$	Sripada et al. (2006)
GSAVI	Green soil adjusted vegetation index	$\frac{\rho_{NIR} - \rho_{Green}}{(\rho_{NIR} + \rho_{Green} + L)} \times (1 + L)$ with $L = 0.5$	

Note: NIR refers to the Near-infrared spectral band. The NIR band was used to calculate the vegetation indices from Sentinel-2 imagery, but it was replaced by the red-edge (RE) spectral band for the vegetation indices calculated from unmanned aerial vehicle imagery.

Statistical analysis

Response variables (epigeous and coprophagous arthropod biomass, as well as biomass of predatory, detritivore, phytophagous, and diverse groups) were log-transformed to achieve linearity, and fixed covariates were z-standardized (mean = 0 and SD = 1). Explanatory variables (season, year, and each VI independently) were tested for collinearity prior to data analysis, and all predictors were retained because all had a generalized variance inflation factor (GVIF) lower than 2 (Fox & Monette, 1992).

We explored fine-scale (UAV) and coarse-scale (S2) relationships between the different groups of arthropod biomass (epigeous and coprophagous, on the one hand, and predatory, detritivore, phytophagous, and diverse on the other) and each of the VIs calculated from UAV and S2 imagery, respectively. For this purpose, we fitted a separate linear regression model (Gaussian error distribution) for each arthropod group (response variable) and each VI (covariate), so that the relationship was evaluated independently for each arthropod group and for each VI. In addition, we incorporated a spatial dependency component to account for potential nonindependence of data collected from nearby sampling stations. This was carried out by incorporating a spatial random effect (i.e., random factor) using integrated nested Laplace approximation with stochastic partial differential equations (INLA-SPDEs) (Lindgren et al., 2011). The spatial dependency of observations was accounted for using a latent Gaussian random field, which we constructed using two-dimensional irregular grids (meshes) based on the geographic coordinates of the

sampling stations. The meshes divided the study area into a large number of nonoverlapping triangles (i.e., Delaunay triangulation) and were employed to approximate the solution of the SPDE that defines the spatial process with a Matérn covariance (Gómez-Rubio, 2020; Zuur et al., 2017). Specifically, we constructed two meshes using the sampling stations at S2 and UAV limits, respectively. The meshes were built using a nonconvex boundary for the coordinates of sampling stations and with a buffer zone in order to avoid edge effects for the bordering vertices (Zuur et al., 2017) (Appendix S4). An independent model was fitted for each VI, incorporating both linear and quadratic forms of the VIs as predictors to control for nonlinear relationships. Orthogonal polynomials were obtained using the function poly from the R package stats (R Core Team, 2020), avoiding high GVIF values and potential collinearity among predictors. Moreover, we incorporated the factors year (2017/2018 for UAV and 2017/2018/2019 for S2) and season (spring/summer/autumn for UAV and winter/spring/summer/autumn for S2) as predictors in order to control for potential inter- and intra-annual variability on epigeous and coprophagous biomass, although no evaluation or discussion of these results is presented (Appendix S5 for these results).

The VIs calculated from UAV and S2 imagery are expected to have a spatial pattern, so spatial confounding might be a problem in our analyses. Spatial confounding occurs when covariates are collinear with the spatial random effects, leading to bias and variance inflation of the fixed effects and, hence, erroneous inference (Hanks et al., 2015; Hodges & Reich, 2010). To overcome this

problem, one potential solution is to constrain the spatial random effect to be orthogonal to those fixed effects with a spatial pattern (Adin et al., 2020; Hodges & Reich, 2010). We tested for spatial confounding in our models by fitting linear regression models incorporating the spatial random intercepts for each observation (response variable) and the VIs as predictors (Hanks et al., 2015). We considered the existence of spatial confounding when the 95% Bayesian Credible Interval (95% BCI) for the VI under consideration did not contain 0, which means that the spatial random intercepts and the VI involved are correlated (see Appendix S6 for results on spatial confounding assessment). In the presence of spatial confounding, we fitted spatial linear regression models (Gaussian error distribution) constraining the spatial random effect to be orthogonal to the VIs (extraconstr argument in INLA; Gómez-Rubio, 2020).

All models were fitted using the R package INLA (Rue et al., 2009) in the free R software (version 4.0.3; R Core Team, 2020). We used INLA default prior distributions for the intercept $\alpha \sim N(0, 0)$, and the regression coefficients $\beta \sim N(0, 1000)$ (Gómez-Rubio, 2020). Parameter estimates were reported as the posterior mean (β), associated SD, and the 95% BCI. We considered predictors to have an effect on the response variable when the parameter's 95% BCI did not overlap zero (Zuur et al., 2017).

RESULTS

VIs calculated from UAV imagery showed higher correlation values (mean \pm SD of the Pearson correlation coefficients = 0.92 ± 0.09) than those calculated from S2 imagery (0.88 ± 0.13 ; see Appendix S7). Moreover, VI

from UAV imagery showed low correlation values with those VI from S2 imagery (0.47 ± 0.09 ; see Appendix S7). Overall, VIs calculated from S2 had higher values than those from UAV imagery (Table 3). All VIs calculated from UAV imagery had higher values in spring than autumn. All S2-derived indices showed their highest values in winter (except for NDVI, which was equal in winter and spring). BNDVI and ENDVI reached their lowest value in summer, GIPVI, GNDVI, GRVI and GSAVI in summer and autumn, and NDVI in autumn (see Appendix S8 for a more detailed description of the inter- and intra-annual variability in the VI).

The biomass of arthropods also varied along the year (Table 4). During the winter we recorded the lowest biomass values per sampling station for all groups, increasing considerably during the spring. In the summer we observed less consistent responses, including negative (predatory and detritivore arthropods), stable (epigeous and diverse arthropods), and positive trends (coprophagous and phytophagous arthropods; Table 4). Most arthropod groups decreased during the autumn except for predatory and phytophagous arthropods that experienced an increase, being the highest values recorded throughout the year for the phytophagous arthropods (Table 4).

Relationship between arthropod biomass and VIs from UAV imagery

All VI from UAV imagery showed a positive linear relationship with the biomass of epigeous arthropods (Table 5, Figure 2). All consumer groups showed a positive relationship with all VI, except for detritivore

TABLE 3 Summary statistics of vegetation indices calculated from unmanned aerial vehicle (UAV) and Sentinel-2 imagery.

Index	UAV			Sentinel-2		
	Mean	SD	Range	Mean	SD	Range
BNDVI	0.15	0.04	[0.08; 0.24]	0.56	0.04	[0.46; 0.66]
ENDVI	0.07	0.03	[0.02; 0.15]	0.43	0.04	[0.34; 0.53]
GIPVI	0.58	0.01	[0.56; 0.62]	0.71	0.02	[0.67; 0.76]
GNDVI	0.17	0.03	[0.12; 0.24]	0.42	0.03	[0.35; 0.51]
GRVI	1.41	0.08	[1.27; 1.62]	2.49	0.20	[2.07; 3.11]
GSAVI	0.25	0.04	[0.18; 0.35]	0.63	0.05	[0.52; 0.77]
NDVI	0.31	0.05	[0.20; 0.48]

Note: The mean, SD, and range [minimum; maximum] are shown. The NDVI index could not be calculated for the UAV imagery because the sensor employed did not provide images along the red spectral band. VI names are provided in Table 2.

Abbreviations: BNDVI, blue normalized difference vegetation index; ENDVI, enhanced normalized difference vegetation index; GIPVI, green infrared percentage vegetation index; GNDVI, green normalized difference vegetation index; GRVI, green ratio vegetation index; GSAVI, green soil adjusted vegetation index; NDVI, normalized difference vegetation index.

TABLE 4 Summary statistics of the biomass of epigeous and coprophagous arthropods as well as the four functional consumer groups (predatory, detritivore, phytophagous and diverse).

Arthropod groups	Winter			Spring			Summer			Autumn		
	Mean	SD	Max	Mean	SD	Max	Mean	SD	Max	Mean	SD	Max
Epigeous	24.1	22.6	114.0	503.0	468.0	3783.7	479.6	381.4	2083.1	379.7	415.5	2666.5
Coprophagous	23.2	68.7	526.9	513.6	1397.2	10219.2	846.8	1519.3	10521.8	687.8	1499.3	9980.8
Predatory	17.8	19.2	96.2	103.7	119.0	1158.9	65.3	65.7	488.8	81.0	141.7	1210.5
Detritivore	0.7	2.1	10.7	164.9	280.7	2424.6	105.9	163.9	1098.8	8.3	19.6	131.8
Phytophagous	4.3	7.0	30.5	155.7	190.0	1404.0	233.8	300.0	1879	262.7	374.4	2555.2
Diverse	0.2	0.6	4.5	67.6	225.0	3434.5	69.5	114.6	1072.8	26.6	116.6	1643.8

Note: The mean, SD, and the maximum value are shown.

TABLE 5 Results of Gaussian spatial models addressing relationship between biomass of epigeous and coprophagous arthropods, and vegetation indices calculated from unmanned aerial vehicle imagery.

Index	Term	β	SD	95% BCI
Epigeous				
BNDVI	Linear	0.345	0.042	[0.261; 0.427]
ENDVI	Linear	0.319	0.043	[0.234; 0.403]
GIPVI	Linear	0.290	0.046	[0.198; 0.381]
GNDVI	Linear	0.290	0.046	[0.198; 0.381]
GRVI	Linear	0.305	0.047	[0.213; 0.397]
GSAVI	Linear	0.289	0.046	[0.198; 0.381]
Coprophagous				
BNDVI	Linear	0.485	0.079	[0.331; 0.639]
ENDVI	Linear	0.503	0.075	[0.355; 0.651]
GIPVI	Linear	0.404	0.089	[0.229; 0.580]
GNDVI	Linear	0.404	0.089	[0.230; 0.578]
GRVI	Linear	0.402	0.090	[0.226; 0.578]
GSAVI	Linear	0.404	0.089	[0.230; 0.579]

Note: Models were fitted using data from 41 sampling stations in spring and autumn 2017 and 48 sampling stations in spring and autumn 2018. Shown are the posterior mean (β), SD, and 95% Bayesian credible interval (95% BCI) for each vegetation index, as well as both the epigeous and coprophagous biomass.

Abbreviations: BNDVI, blue normalized difference vegetation index; ENDVI, enhanced normalized difference vegetation index; GIPVI, green infrared percentage vegetation index; GNDVI, green normalized difference vegetation index; GRVI, green ratio vegetation index; GSAVI, green soil adjusted vegetation index.

arthropods that did not show any relationship with ENDVI index and for diverse arthropods which did not show any relationship with GRVI index (see Appendix S9 for arthropod group results). Lastly, all VI calculated from UAV imagery showed a positive linear relationship with the biomass of coprophagous arthropods (Table 5, Figure 3).

Relationship between arthropod biomass and VIs from Sentinel-2 imagery

In the case of the VIs calculated from the S2 imagery, not all VIs showed a relationship with the biomass of epigeous and coprophagous arthropods. The NDVI calculated from S2 imagery showed a negative relationship with the biomass of epigeous arthropods (Figure 4). The BNDVI and the ENDVI were positively correlated with epigeous biomass (both linear and quadratic terms; Table 6, Figure 4), whereas the remaining indices showed no relationship with epigeous biomass (Table 6). Regarding the biomass of each consumer group we observed that ENDVI and BNDVI were positively correlated with the biomass of predatory, detritivore, and diverse arthropods but not for the biomass of phytophagous arthropods. Moreover, the NDVI was negatively correlated with the biomass of phytophagous arthropods, but not with the other consumer groups. All other VIs were only positively correlated with the biomass of predatory arthropods (see Appendix S9 for these results). Lastly, all VIs were positively correlated with coprophagous biomass, except for the NDVI, which showed no relationship (Table 6, Figure 5).

DISCUSSION

Information about ecological patterns and processes at large spatial scales is essential for both basic and applied studies. However, the effort required to field-collect this type of data may be unaffordable, especially for some specific organisms, and its applicability at large spatial scales can then be restricted. Thus, the use of remote sensing imagery to search and map natural processes at large or very large spatial scales offers great possibilities. This work has shown a solid positive relationship between different remote sensing-derived VI and arthropod biomass, even after accounting for seasonal and interannual

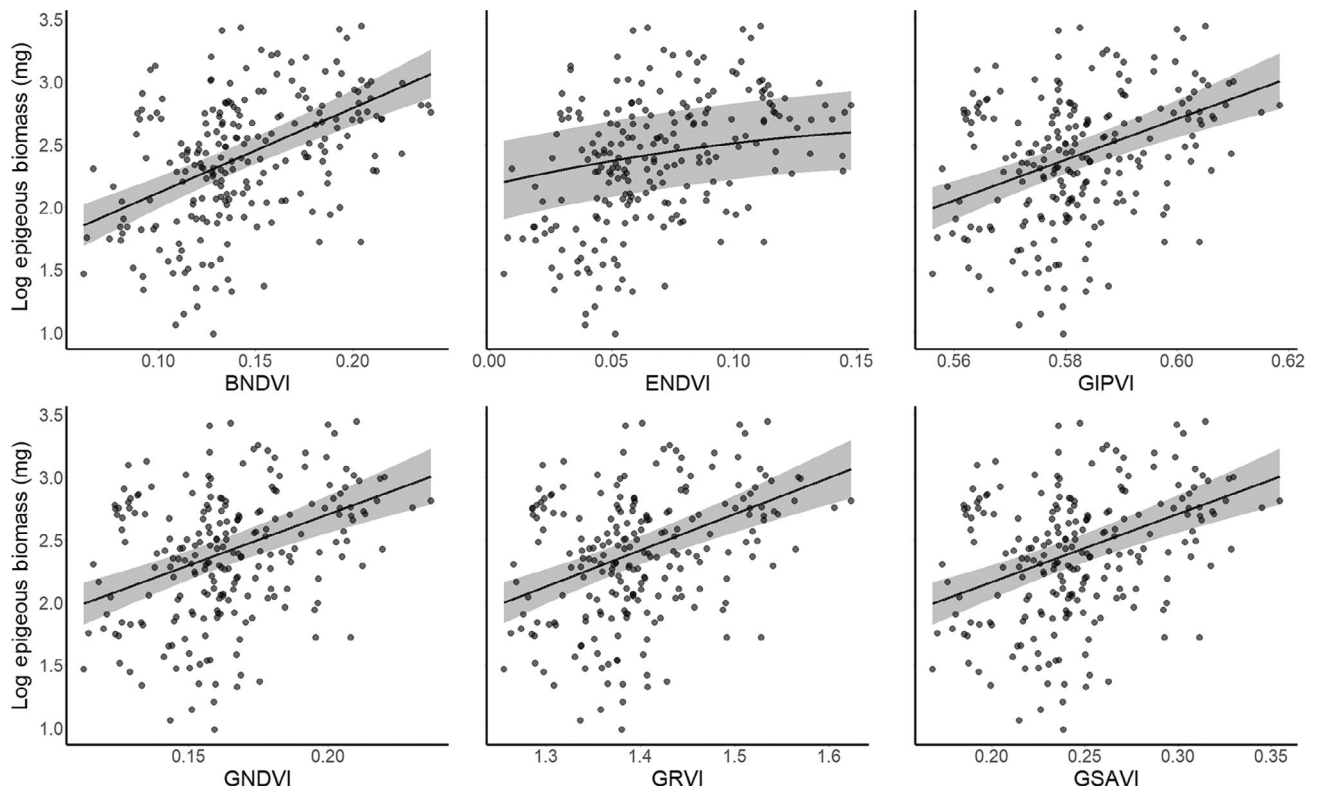


FIGURE 2 Relationship between biomass of epigeous arthropods and vegetation indices calculated from unmanned aerial vehicle imagery. The mean (black line) and 95% Bayesian credible interval (95% BCI; gray surface) of the values predicted by the models are shown, as are the observation values for each sampling station (points). BNDVI, blue normalized difference vegetation index; ENDVI, enhanced normalized difference vegetation index; GIPVI, green infrared percentage vegetation index; GNDVI, green normalized difference vegetation index; GRVI, green ratio vegetation index; GSAVI, green soil adjusted vegetation index.

variability and geographic position. This relationship was especially strong and consistent when working with fine-scale UAV-derived VI, but it was also found with several coarser-scale S2-derived VIs, which consequently suggests a strong capacity to use raster imagery to extrapolate information on unexplored or nonsampled areas.

Despite the difference in channels used for estimating VIs between UAV and S2 imagery, our results seem conclusive about the relationship between VIs and arthropod biomass. Indeed, both VIs calculated from the NIR and the RE bands in our sampling stations located in shrub steppes were highly correlated, and consequently, modeling results using RE were basically the same as those using NIR and presented in the [Results](#) section (Appendix S3). Thus, we consider that our results are solid regardless of the channel used. Our results are in agreement with those of several previous works carried out on different habitat types that found a strong correlation between S2 RE- and NIR-derived VIs, though the former were less affected by plant traits, especially when assessing temporal variation (Fernández-Tizón et al., 2020; Imran et al., 2020; Sweet et al., 2015; Upadhyay et al., 2013).

Our results showed a strong relationship between all UAV-derived VIs and epigeous arthropod biomass

(see also results on consumer functional groups in Appendix S9). In the case of S2-derived VIs, however, only two VIs (BNDVI and ENDVI) showed a positive relationship with the biomass of epigeous arthropods, whereas one VI (NDVI) showed a negative relationship, which could be primarily driven by the negative relationship observed between phytophagous arthropods and S2-derived NDVI (Appendix S9). These differences between VIs might be explained by the observed discrepancies in the intra-annual variation of the S2-derived VIs, with autumn being the season in which these discrepancies were most evident (Appendix S8). The S2-derived BNDVI and ENDVI increased in autumn, whereas GIPVI, GNDVI, GRVI, and GSAVI remained stable, and NDVI decreased compared to the summer values (Appendix S8). Future research should address the relationship between field measurements of plant productivity and VI values to better understand the discrepancies observed between S2-derived VIs and to elucidate which index is the best indicator of plant productivity in shrub steppes and, thus, of arthropod biomass.

The highest performance of UAV versus S2-derived VIs to correlate with arthropod biomass may be explained by differences in spatial resolution. UAV-derived VIs were

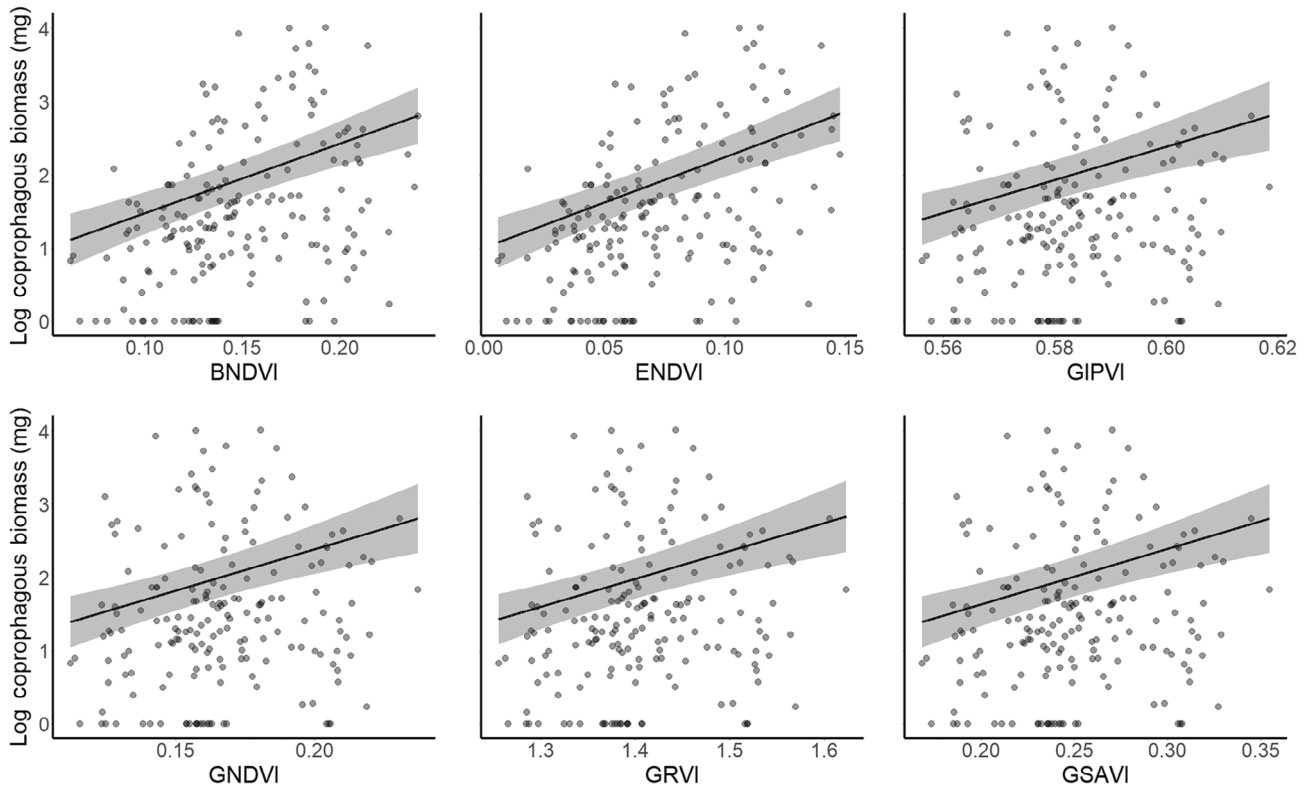


FIGURE 3 Relationship between biomass of coprophagous arthropods and vegetation indices calculated from unmanned aerial vehicle imagery. The mean (black line) and 95% Bayesian credible interval (95% BCI; gray surface) of the values predicted by the models are shown, as are the observation values for each sampling station (points). BNDVI, blue normalized difference vegetation index; ENDVI, enhanced normalized difference vegetation index; GIPVI, green infrared percentage vegetation index; GNDVI, green normalized difference vegetation index; GRVI, green ratio vegetation index; GSAVI, green soil adjusted vegetation index.

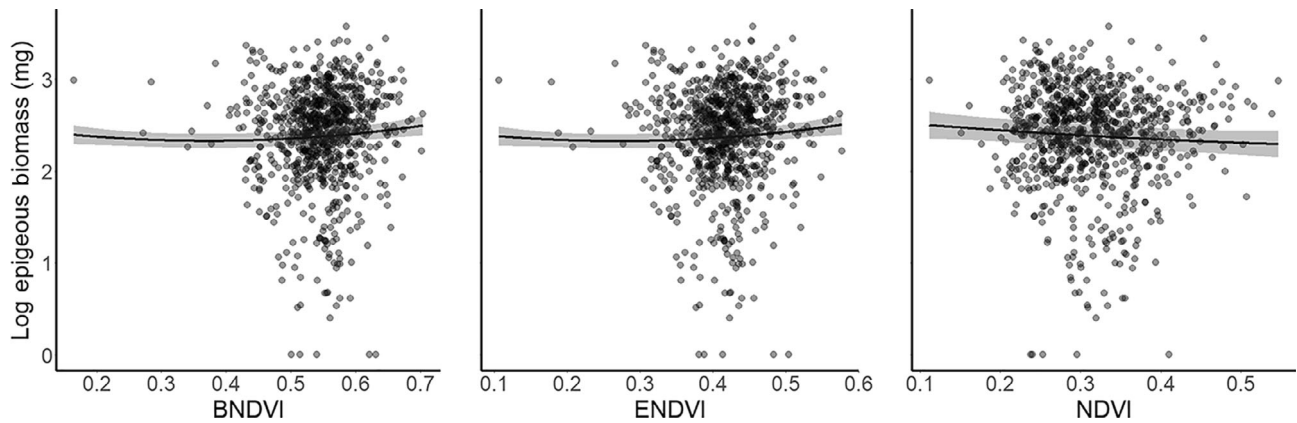


FIGURE 4 Relationship between biomass of epigeous arthropods and vegetation indices calculated from Sentinel-2 imagery. The mean (black line) and 95% Bayesian credible interval (95% BCI; gray surface) of the values predicted by the models are shown, as are the observation values for each sampling station (points). BNDVI, blue normalized difference vegetation index; ENDVI, enhanced normalized difference vegetation index; NDVI, normalized difference vegetation index.

calculated at a 50-cm resolution (after downscaling from the initial 4-cm resolution), whereas S2-derived VIs were at a 10-m resolution. The same reasoning might also be valid for explaining the differences among the VI values estimated using UAV and S2 since the values of the

same index greatly differ with the approach employed. In the case of epigeous arthropod biomass, a small spatial-scale relationship with vegetation could be expected (Báldi & Kisbenedek, 1997; Labadessa et al., 2015; Weyer et al., 2012) because epigeous arthropods include species

TABLE 6 Results of Gaussian spatial models addressing relationship between the biomass of epigeous and coprophagous arthropods, and vegetation indices calculated from Sentinel-2 imagery.

Index	Term	β	SD	95% BCI
Epigeous				
BNDVI	Linear	0.029	0.015	[0.001; 0.058]
	Quadratic	0.033	0.013	[0.007; 0.059]
ENDVI	Linear	0.037	0.014	[0.008; 0.065]
	Quadratic	0.034	0.013	[0.008; 0.060]
GIPVI	Linear	-0.006	0.043	[-0.091; 0.079]
GNDVI	Linear	-0.006	0.043	[-0.091; 0.079]
GRVI	Linear	0.005	0.039	[-0.071; 0.082]
GSAVI	Linear	-0.006	0.043	[-0.091; 0.079]
NDVI	Linear	-0.130	0.041	[-0.211; -0.049]
Coprophagous				
BNDVI	Linear	0.439	0.115	[0.213; 0.664]
ENDVI	Linear	0.441	0.105	[0.234; 0.648]
GIPVI	Linear	0.261	0.118	[0.030; 0.492]
GNDVI	Linear	0.261	0.118	[0.030; 0.492]
GRVI	Linear	0.211	0.107	[0.001; 0.422]
GSAVI	Linear	0.261	0.118	[0.030; 0.492]
NDVI	Linear	-0.091	0.111	[-0.309; 0.126]

Note: Models were fitted using data from 79 sampling stations in spring, summer and autumn 2017, and 67 sampling stations in spring, summer, and autumn 2018 and 2019, and winter 2019. Shown are the posterior mean (β), SD, and 95% Bayesian credible interval (95% BCI) for each vegetation index, as well as both the epigeous and coprophagous biomass.

Abbreviations: BNDVI, blue normalized difference vegetation index; ENDVI, enhanced normalized difference vegetation index; GIPVI, green infrared percentage vegetation index; GNDVI, green normalized difference vegetation index; GRVI, green ratio vegetation index; GSAVI, green soil adjusted vegetation index; NDVI, normalized difference vegetation index.

both sedentary and of some mobility (Dennis et al., 1998). Thus, the relationship may be more difficult to identify when spatial resolution is coarser (see, however, Fernández-Tizón et al., 2020). Changes in spatial resolution, as mentioned earlier, can modify the determination coefficient of greenness indices, thereby changing the greenness values of each pixel (Díaz-Delgado et al., 2017; Prabhakara et al., 2015). Another complementary explanation could help to shed light on the differences between the UAV and S2 results. The chlorophyll absorption range is usually between 400 and 700 nm (Ollinger, 2011), though in our case UAV-derived VIs used the RE channel, which is above 700 nm. However, S2-derived VIs estimated with the RE channel showed similar results (Appendix S3), which suggests that changes should be linked to spatial resolution more than to radiometric effects. In any case, more research is needed in this sense in order to disentangle which

radiometrically detected elements are related to arthropod activity and biomass.

We found a strong and consistently positive relationship between epigeous arthropod biomass and vegetation, except for S2-derived NDVI. Arthropods seem to be an especially suitable group to be correlated with plant productivity because their response to changes in plant community are faster than those of vertebrates (Thomas et al., 2004). Previous works also found strong, although not always linear, relationships between arthropod abundance or biomass and plant traits related with productivity, such as size, plant condition, or leaf area (e.g., Fernández-Tizón et al., 2020, Harrison et al., 2018, Prather & Kaspari, 2019, Smith et al., 2020, Sweet et al., 2015). In summary, increases in plant productivity promote a higher abundance of arthropod herbivores (Carmona et al., 2011; Smith et al., 2020), which in turn increases arthropod predator and parasite populations (Langellotto & Denno, 2004; Prather & Kaspari, 2019; Smith et al., 2020). In our case, predatory arthropods showed a positive linear relationship with all VIs (except for the NDVI), whereas detritivore and diverse arthropods showed positive relationships with the S2-derived BNDVI and ENDVI. However, phytophagous arthropods showed a negative relationship with S2-derived NDVI (Appendix S9). In the case of S2-derived NDVI, our results are counterintuitive; we expected a similar positive relationship like that found in the other VIs. This may be because phytophagous arthropod biomass reaches its maximum values in autumn and minimum values in winter (Table 4), when the NDVI reaches its minimum and maximum values, respectively (Appendix S8). In any case, in shrub-steppe habitats where bare ground cover is especially high and shrubs with pointed and thin leaves predominate (Zurdo et al., 2021), NDVI seems to show an inverse behavior compared with green channel-based VIs, perhaps due to its higher level of reflectance for green wavelengths (Gitelson et al., 1996; Sripada et al., 2006). In a previous work, Sweet et al. (2015) showed that estimates of NDVI calculated at 1-m² quadrats by a field portable spectroradiometer correlated positively with arthropod biomass. Fernández-Tizón et al. (2020) found a positive significant relationship between satellite-derived NDVI and arthropod biomass in semi-natural grasslands in central Europe, though the spatial resolution of the satellite imagery was much coarser than ours (16 × 16 km), so it had a lower extrapolation capacity. None of the aforementioned works, in addition to our own, showed relationships with a maximum between VIs and biomass, suggesting that the maximums are probably outside of the studied indices (habitats). Despite the remarkable utility of satellite-derived VIs (and specially NDVI) in animal ecology (Pettorelli

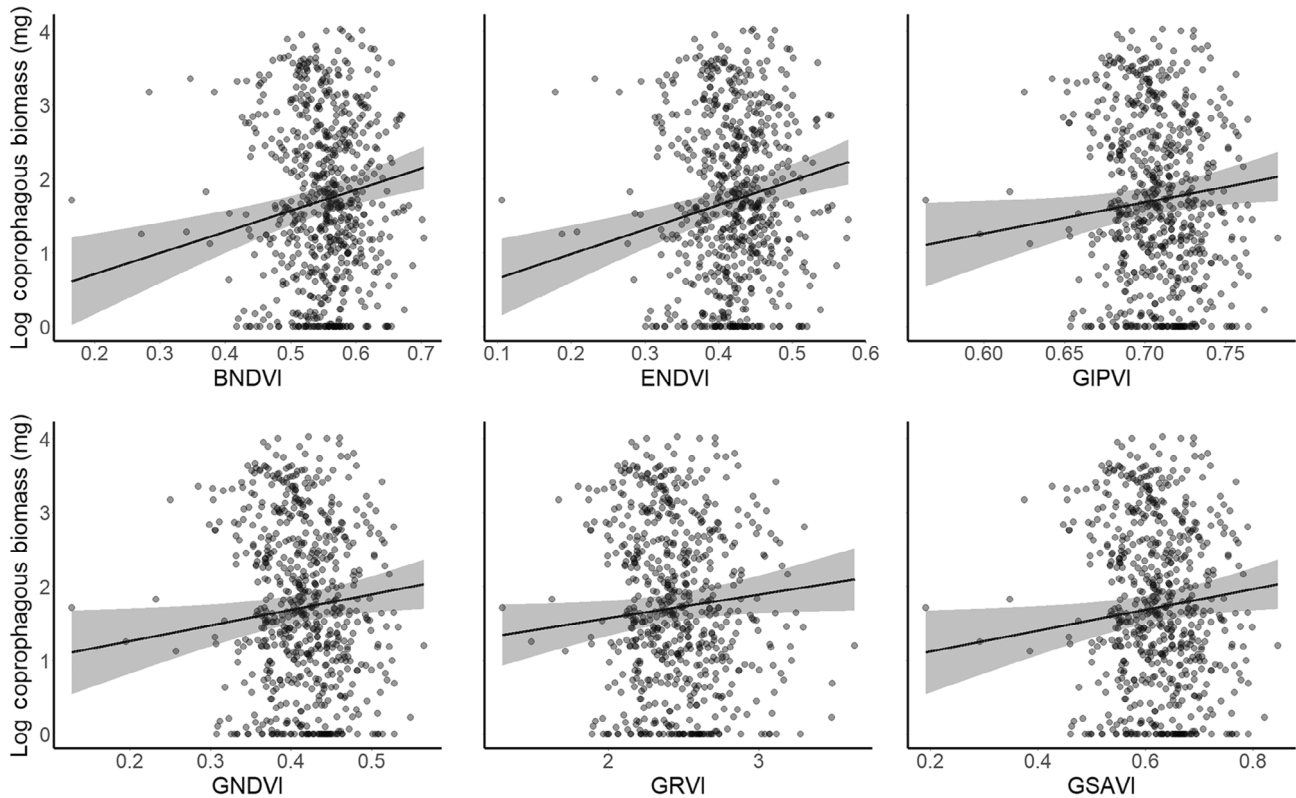


FIGURE 5 Relationship between biomass of coprophagous arthropods and vegetation indices calculated from Sentinel-2 imagery. The mean (black line) and 95% Bayesian credible interval (95% BCI; gray surface) of the values predicted by the models are shown, as are the observation values for each sampling station (points). BNDVI, blue normalized difference vegetation index; ENDVI, enhanced normalized difference vegetation index; GIPVI, green infrared percentage vegetation index; GNDVI, green normalized difference vegetation index; GRVI, green ratio vegetation index; GSAVI, green soil adjusted vegetation index.

et al., 2011), our results suggest the need for more study of the differences between VIs and their relationships with biodiversity elements.

All UAV-derived and almost all S2-derived VIs, except for NDVI, showed a positive relationship with the biomass of coprophagous arthropods. The coprophagous group includes high-mobility species that are attracted to a baited trap, sometimes from long distances (Dormont et al., 2007; Perrin et al., 2019) and independently of the characteristics of the above-ground vegetation where the trap is located. Our results, being so solid for both UAV and S2, suggest that a coprophagous species pool attracted to a baited trap might be highly local and dependent on other exogenous factors as the abundance of dung of herbivorous mammals. Extensive sheep grazing, as well as the abundance of wild herbivores, is probably more intense where plant productivity is higher. Then, in a circular way, plant productivity is expected to be higher at sites where dung-processing arthropods are more abundant because their activity increases nutrient content in the soil (Prather & Kaspari, 2019).

A remarkable result of this work is the high degree of similarity among the VIs in their relationship with arthropod biomass. In the case of UAV-derived VIs, they all showed a linear relationship with both epigeous and coprophagous arthropod biomass. In the case of S2-derived VIs, the relationship was not as obvious or linear for epigeous arthropod biomass but much more evident and linear for the case of coprophagous arthropod biomass. Since the proposal of the first VIs, including NDVI (Rouse et al., 1974), a very large number of remote sensing-derived indices exploring plant productivity, biomass, health, and vigor have been put forth. Many of them rely on the relation between NIR or RE and the visual range of the spectrum, posing the differences in the distinctive absorbance spectrum of chlorophyll between red (or blue or green) and NIR (or RE) regions. As in other cases (e.g., Viña et al., 2011), our comparison of VIs yielded inconclusive results with respect to selecting the best index but, on the contrary, suggests that almost all the indices performed satisfactorily in terms of predicting arthropod biomass, except for NDVI, despite being the most commonly used index. In any case, our

results are most probably habitat-dependent (Weiss et al., 2013), and extrapolations for different habitats/regions should include previous ground-truth fieldwork. Iberian steppe habitats are not especially productive because they are subject to a high thermal range, with extremely low winter temperatures and high summer temperatures, low annual precipitation, and frequently in the form of snow (Aranbarri et al., 2015). Under these conditions, positive relationships between arthropod biomass and VIs may be expected.

CONCLUSION

Our results show that remote sensing imagery and the derived VIs may perform satisfactorily as proxies of arthropod biomass in shrub steppes. We found slight differences between VIs in their general performance in terms of explaining arthropod biomass. If considering the potential of close site dependence of our results, the selection of the optimal VI would depend on prior calibration between remote and field data. At any rate, our results showed that all the UAV-derived VIs evaluated performed satisfactorily for estimating arthropod biomass. In the case of S2-derived VIs, only BNDVI and ENDVI performed well in the case of epigeous biomass, and all but NDVI performed well in the case of coprophagous biomass. Thus, if a particular index must be chosen, we suggest using BNDVI or ENDVI because they were the only two indices that showed strong and consistent correlations for all the arthropod groups and spatial resolutions tested. Though low-cost UAVs are in constant development, the total expenses incurred from using UAVs are difficult to estimate and frequently are ultimately not very low (Jiménez López & Mulero-Pázmány, 2019), especially if the study area is large. In those cases, we recommend using Sentinel free imagery and BNDVI or ENDVI as a proxy of arthropod biomass in shrub steppes, after the relationship is adequately calibrated, especially in remote or unsampled areas. Arthropod biomass seems to be positively correlated with plant biomass and vigor, which in turn may benefit from natural fertilization from extensive grazing. Thus, maintenance of extensive sheep grazing should result in increased arthropod biomass and diversity and, consequently, in healthier populations of insectivorous birds.

AUTHOR CONTRIBUTIONS

J. Traba and E. L. García de la Morena conceived the original idea, and J. Traba supervised the project. J. Traba and I. Hervás secured funding. J. Gómez-Catasús curated and analyzed the data. A. Barrero, D. Bustillo-de la Rosa, M. Reverter, and J. Gómez-Catasús prepared the

original databases. A. Barrero and E.L. García de la Morena calculated the VIs from UAV imagery, D. Bustillo-de la Rosa calculated the VIs from S2 imagery, and M. Reverter and J. Zurdo carried out lab work. J. Gómez-Catasús, A. Barrero, D. Bustillo-de la Rosa, J. Zurdo, C. Pérez-Granados, A. Santamaría, and M. Reverter carried out field work. E. L. García de la Morena performed drone flights and prepared raster data. J. Traba and J. Gómez-Catasús took the lead in writing the manuscript, and all authors provided critical feedback and contributed to the final manuscript.

ACKNOWLEDGMENTS

Many people have collaborated over the course of all these years in field data collection and lab-processing samples. We wish to thank Inmaculada Abril-Colón, Ana Santos, Filipino Colla, Álvaro Ortega, Miguel Muñoz, and Adaia Cid. We also thank Juan Corley and two anonymous reviewers whose comments helped to improve the manuscript. This study was partially supported by the European Commission (Life Ricotí Project LIFE15-NAT-ES-000802 and Life Connect Ricotí Project LIFE20-NAT-ES-000133) and the BBVA Foundation (BBVA-Dron Ricotí project). This paper contributes to the REMEDINAL-3 project from Community of Madrid.

CONFLICT OF INTEREST

The authors declare no conflict of interest.

DATA AVAILABILITY STATEMENT


All data and R-code (Gomez-Catasus, 2022) are available on Zenodo at <https://doi.org/10.5281/zenodo.6621453>.

ORCID


J. Traba  <https://orcid.org/0000-0001-6326-8942>

J. Gómez-Catasús  <https://orcid.org/0000-0001-8949-5318>

A. Barrero  <https://orcid.org/0000-0002-2980-1202>

D. Bustillo-de la Rosa  <https://orcid.org/0000-0002-8584-2834>

J. Zurdo  <https://orcid.org/0000-0002-7283-3322>

C. Pérez-Granados  <https://orcid.org/0000-0003-3247-4182>

E. L. García de la Morena  <https://orcid.org/0000-0001-6746-4414>

A. Santamaría  <https://orcid.org/0000-0001-8376-0969>

M. Reverter  <https://orcid.org/0000-0003-0979-871X>

REFERENCES

- Adin, A., T. Goicoa, J. S. Hodges, P. Schnell, and M. D. Ugarte. 2020. "Alleviating Confounding in Spatio-Temporal Areal Models with an Application on Crimes against Women in India." arXiv:2003.01946.

- Aranbarri, J., P. González-Sampériz, E. Iriarte, A. Moreno, M. Rojo-Guerra, L. Peña-Chocarro, B. Valero-Garcés, et al. 2015. "Human-Landscape Interactions in the Conquezuela-Ambrona Valley (Soria, Continental Iberia): From the Early Neolithic Land Use to the Origin of the Current Oak Woodland." *Palaeogeography, Palaeoclimatology, Palaeoecology* 436: 41–57.
- Báldi, A., and T. Kisbenedek. 1997. "Orthopteran Assemblages as Indicators of Grassland Naturalness in Hungary." *Agriculture, Ecosystems and Environment* 66: 121–9.
- Belgiu, M., and O. Csillik. 2018. "Sentinel-2 Cropland Mapping Using Pixel-Based and Object-Based Time-Weighted Dynamic Time Warping Analysis." *Remote Sensing of Environment* 204: 509–23.
- Carmona, D., M. J. Lajeunesse, and M. T. J. Johnson. 2011. "Plant Traits that Predict Resistance to Herbivores." *Functional Ecology* 25: 358–67.
- Colomina, I., and P. Molina. 2014. "Unmanned Aerial Systems for Photogrammetry and Remote Sensing: A Review." *ISPRS Journal of Photogrammetry and Remote Sensing* 92: 79–97.
- Crippen, R. E. 1990. "Calculating the Vegetation Index Faster." *Remote Sensing of Environment* 34: 71–3.
- Dennis, P., M. R. Young, and I. J. Gordon. 1998. "Distribution and Abundance of Small Insects and Arachnids in Relation to Structural Heterogeneity of Grazed, Indigenous Grasslands." *Ecological Entomology* 23: 253–64.
- Díaz-Delgado, R., C. Hurford, and R. Lucas. 2017. "Introducing the Book 'the Roles of Remote Sensing in Nature Conservation.'" In *The Roles of Remote Sensing in Nature Conservation*, edited by R. Díaz-Delgado, R. Lucas, and C. Hurford, 3–10. Cham: Springer.
- Dormont, L., S. Rapior, D. B. McKey, and J. P. Lumaret. 2007. "Influence of Dung Volatiles on the Process of Resource Selection by Coprophagous Beetles." *Chemoecology* 17: 23–30.
- Fernández-Tizón, M., T. Emmenegger, J. Perner, and S. Hahn. 2020. "Arthropod Biomass Increase in Spring Correlates with NDVI in Grassland Habitat." *Science of Nature* 107: 1–7.
- Fox, J., and G. Monette. 1992. "Generalized collinearity diagnostics." *Journal of the American Statistical Association* 87: 178–83.
- Fraser, R. H., J. van der Sluijs, and R. J. Hall. 2017. "Calibrating Satellite-Based Indices of Burn Severity from UAV-Derived Metrics of a Burned Boreal Forest in NWT, Canada." *Remote Sensing* 9: 279.
- Gitelson, A. A., Y. J. Kaufman, and M. N. Merzlyak. 1996. "Use of a Green Channel in Remote Sensing of Global Vegetation from EOS-MODIS." *Remote Sensing of Environment* 58: 289–98.
- Gómez-Catasús, J., V. Garza, M. B. Morales, and J. Traba. 2019. "Hierarchical Habitat-Use by an Endangered Steppe Bird in Fragmented Landscapes Is Associated with Large Connected Patches and High Food Availability." *Scientific Reports* 9: 1–12.
- Gómez-Rubio, V. 2020. *Bayesian Inference with INLA*. Boca Raton, FL: Chapman & Hall/CRC Press.
- Haddad, N. M., D. Tilman, J. Haarstad, M. Ritchie, and J. M. H. Knops. 2001. "Contrasting Effects of Plant Richness and Composition on Insect Communities: A Field Experiment." *American Naturalist* 158: 17–35.
- Hanks, E. M., E. M. Schliep, M. B. Hooten, and J. A. Hoeting. 2015. "Restricted Spatial Regression in Practice: Geostatistical Models, Confounding, and Robustness under Model Misspecification." *Environmetrics* 26: 243–54.
- Harrison, J. G., C. S. Philbin, Z. Gompert, G. W. Forister, L. Hernandez-Espinoza, B. W. Sullivan, I. S. Wallace, et al. 2018. "Deconstruction of a Plant-Arthropod Community Reveals Influential Plant Traits with Nonlinear Effects on Arthropod Assemblages." *Functional Ecology* 32: 1317–28.
- Hódar, J. A. 1996. "The Use of Regression Equations for Estimation of Arthropod Biomass in Ecological Studies." *Acta Oecologica* 17: 421–33.
- Hodges, J. S., and B. J. Reich. 2010. "Adding Spatially-Correlated Errors Can Mess up the Fixed Effect you Love." *American Statistician* 64: 325–34.
- Huete, A. R., H. Q. Liu, K. Batchily, and W. Van Leeuwen. 1997. "A Comparison of Vegetation Indices over a Global Set of TM Images for EOS-MODIS." *Remote Sensing of Environment* 59: 440–51.
- Hunt, E. R., W. Dean Hively, S. J. Fujikawa, D. S. Linden, C. S. T. Daughtry, and G. W. McCarty. 2010. "Acquisition of NIR-Green-Blue Digital Photographs from Unmanned Aircraft for Crop Monitoring." *Remote Sensing* 2: 290–305.
- Imran, H. A., D. Gianelle, D. Rocchini, M. Dalponte, M. P. Martín, K. Sakowska, G. Wohlfahrt, and L. Vescovo. 2020. "VIS-NIR, Red-Edge and NIR-Shoulder Based Normalized Vegetation Indices Response to Co-Varying Leaf and Canopy Structural Traits in Heterogeneous Grasslands." *Remote Sensing* 12: 2254.
- Inglada, J., M. Arias, B. Tardy, O. Hagolle, S. Valero, D. Morin, G. Dedieu, et al. 2015. "Assessment of an Operational System for Crop Type Map Production Using High Temporal and Spatial Resolution Satellite Optical Imagery." *Remote Sensing* 7: 12356–79.
- Gomez-Catasus, J. 2022. "Primary-Productivity-Correlates-with-Arthropod-Biomass-Comparing-Satellite--and-Drone-Based-Vegetat: Comparative Assessment of Satellite- and Drone-Based Vegetation Indices to Predict Arthropod Biomass in Shrub-Steppes (v.1.0.0)." Zenodo. <https://doi.org/10.5281/zenodo.6621453>.
- Jiménez López, J., and M. Mulero-Pázmány. 2019. "Drones for Conservation in Protected Areas: Present and Future." *Drones* 3: 10.
- Kaspari, M., M. Yuan, and L. Alonso. 2003. "Spatial Grain and the Causes of Regional Diversity Gradients in Ants." *American Naturalist* 161: 459–77.
- Kross, A., H. McNairn, D. Lapen, M. Sunohara, and C. Champagne. 2015. "Assessment of RapidEye Vegetation Indices for Estimation of Leaf Area Index and Biomass in Corn and Soybean Crops." *International Journal of Applied Earth Observation and Geoinformation* 34: 235–48.
- Labadessa, R., L. Forte, and P. Mairota. 2015. "Exploring Life Forms for Linking Orthopteran Assemblage and Grassland Plant Community." *Hacquetia* 14: 33–42.
- Langelotto, G. A., and R. F. Denno. 2004. "Responses of Invertebrate Natural Enemies to Complex-Structured Habitats: A Meta-Analytical Synthesis." *Oecologia* 139: 1–10.
- Lebourgeois, V., A. Bégué, S. Labbé, B. Mallavan, L. Prévot, and B. Roux. 2008. "Can Commercial Digital Cameras Be Used as Multispectral Sensors? A Crop Monitoring Test." *Sensors* 8: 7300–22.

- Lindgren, F., H. Rue, and J. Lindström. 2011. "An Explicit Link between Gaussian Fields and Gaussian Markov Random Fields: The Stochastic Partial Differential Equation Approach." *Journal of the Royal Statistical Society. Series B: Statistical Methodology* 73: 423–98.
- Losey, J. E., and M. Vaughan. 2006. "The Economic Value of Ecological Services Provided by Insects." *Bioscience* 56: 311–23.
- Möller, M., H. Gerstmann, F. Gao, T. C. Dahms, and M. Förster. 2017. "Coupling of Phenological Information and Simulated Vegetation Index Time Series: Limitations and Potentials for the Assessment and Monitoring of Soil Erosion Risk." *Catena* 150: 192–205.
- Ollinger, S. V. 2011. "Sources of Variability in Canopy Reflectance and the Convergent Properties of Plants." *New Phytologist* 189: 375–94.
- Perrin, W., P. Jay-Robert, B. Buatois, and L. Tatin. 2019. "A Comparative Analysis of Dung Beetle Assemblages (Coleoptera: Scarabaeidae: Scarabaeinae, Aphodiinae) Attracted to Sheep and Little Bustard Excrement in Southern France." *The Coleopterists Bulletin* 73: 185–92.
- Pettorelli, N., S. Ryan, T. Mueller, N. Bunnefeld, B. Jedrzejewska, M. Lima, and K. Kausrud. 2011. "The Normalized Difference Vegetation Index (NDVI): Unforeseen Successes in Animal Ecology." *Climate Research* 46: 15–27.
- Pla, M., G. Bota, A. Duane, J. Balagué, A. Curcó, R. Gutiérrez, and L. Brotons. 2019. "Calibrating Sentinel-2 Imagery with Multi-spectral UAV Derived Information to Quantify Damages in Mediterranean Rice Crops Caused by Western Swamphen (*Porphyrio porphyrio*)." *Drones* 3: 45.
- Prabhakara, K., W. Dean Hively, and G. W. McCarty. 2015. "Evaluating the Relationship between Biomass, Percent Groundcover and Remote Sensing Indices across Six Winter Cover Crop Fields in Maryland, United States." *International Journal of Applied Earth Observation and Geoinformation* 39: 88–102.
- Prather, R. M., and M. Kaspari. 2019. "Plants Regulate Grassland Arthropod Communities through Biomass, Quality, and Habitat Heterogeneity." *Ecosphere* 10: e02909.
- Quantum GIS Development Team. 2020. "Quantum GIS Geographic Information System." Open Source Geospatial Foundation Project. <http://qgis.osgeo.org>.
- R Core Team. 2020. *R: A Language and Environment for Statistical Computing*. Vienna: R Foundation for Statistical Computing <http://www.r-project.org>.
- Rasmussen, J., G. Ntakos, J. Nielsen, J. Svendsgaard, R. N. Poulsen, and S. Christensen. 2016. "Are Vegetation Indices Derived from Consumer-Grade Cameras Mounted on UAVs Sufficiently Reliable for Assessing Experimental Plots?" *European Journal of Agronomy* 74: 75–92.
- Reverter, M., J. Gómez-Catasús, A. Barrero, C. Pérez-Granados, D. Bustillo-de La Rosa, and J. Traba. 2019. "Interactions in Shrubsteppes: Implications for the Maintenance of a Threatened Bird." *Ecosistemas: Revista Científica y Técnica de Ecología y Medio Ambiente* 28: 69–77.
- Reverter, M., J. Gómez-Catasús, A. Barrero, and J. Traba. 2021. "Crops Modify Habitat Quality beyond their Limits." *Agriculture, Ecosystems & Environment* 319: 107542.
- Rouse, J. W., R. H. Haas, J. A. Schell, and D. W. Deering. 1974. "Monitoring Vegetation Systems in the Great Plains with ERTS." *NASA Special Publication* 351: 309–17.
- Rue, H., S. Martino, and N. Chopin. 2009. "Approximate Bayesian Inference for Latent Gaussian Models by Using Integrated Nested Laplace Approximations." *Journal of the Royal Statistical Society. Series B: Statistical Methodology* 71: 319–92.
- Sainz Ollero, H. 2013. "Steppes across the World: An Overview with Emphasis on the Iberian Peninsula." In *Steppe Ecosystems: Biological Diversity, Management and Restoration*, edited by M. B. Morales and J. Traba, 1–25. New York, NY: NOVA Science Publishers.
- Sainz Ollero, H., and M. A. van Staalduinen. 2012. "Iberian Steppes." In *Eurasian Steppes: Ecological Problems and Livelihoods in a Changing World*, edited by M. J. A. Werger and M. A. van Staalduinen, 273–88. London: Springer.
- Salamí, E., C. Barrado, and E. Pastor. 2014. "UAV Flight Experiments Applied to the Remote Sensing of Vegetated Areas." *Remote Sensing* 6: 11051–81.
- Sardà-Palomera, F., G. Bota, C. Viñolo, O. Pallarés, V. Sazatornil, L. Brotons, S. Gomáriz, and F. Sardà. 2012. "Fine-Scale Bird Monitoring from Light Unmanned Aircraft Systems." *Ibis* 154: 177–83.
- Serrano, L., J. A. Gamon, and J. Penuelas. 2000. "Estimation of Canopy Photosynthetic and Nonphotosynthetic Components from Spectral Transmittance." *Ecology* 81: 3149–62.
- Siemann, E. 1998. "Experimental Tests of Effects of Plant Productivity and Diversity on Grassland Arthropod Diversity." *Ecology* 79: 2057–70.
- Smith, B. M., N. J. Aebischer, J. Ewald, S. Moreby, C. Potter, and J. M. Holland. 2020. "The Potential of Arable Weeds to Reverse Invertebrate Declines and Associated Ecosystem Services in Cereal Crops." *Frontiers in Sustainable Food Systems* 3: 118.
- Southwood, T. R. E., V. K. Brown, and P. M. Reader. 1979. "The Relationships of Plant and Insect Diversities in Succession." *Biological Journal of the Linnean Society* 12: 327–48.
- Sripada, R. P., R. W. Heiniger, J. G. White, and A. D. Meijer. 2006. "Aerial Color Infrared Photography for Determining Early in-Season Nitrogen Requirements in Corn." *Agronomy Journal* 98: 968–77.
- Srivastava, D. S., and J. H. Lawton. 1998. "Why more Productive Sites Have More Species: An Experimental Test of Theory Using Tree-Hole Communities." *American Naturalist* 152: 510–29.
- Strong, C. J., N. G. Burnside, and D. Llewellyn. 2017. "The Potential of Small-Unmanned Aircraft Systems for the Rapid Detection of Threatened Unimproved Grassland Communities Using an Enhanced Normalized Difference Vegetation Index." *PLoS One* 12: e0186193.
- Sweet, S. K., A. Asmus, M. E. Rich, J. Wingfield, L. Gough, and N. T. Boelman. 2015. "NDVI as a Predictor of Canopy Arthropod Biomass in the Alaskan Arctic Tundra." *Ecological Applications* 25: 779–90.
- Thomas, J. A., M. G. Telfer, D. B. Roy, C. D. Preston, J. J. D. Greenwood, J. Asher, R. Fox, R. T. Clarke, and J. H. Lawton. 2004. "Comparative Losses of British Butterflies, Birds, and Plants and the Global Extinction Crisis." *Science* 303: 1879–81.
- Traba, J., M. B. Morales, E. L. García De La Morena, M. P. Delgado, and A. Krištín. 2007. "Selection of Breeding Territory by Little Bustard (*Tetrax tetrax*) Males in Central Spain: The Role of Arthropod Availability." *Ecological Research* 23: 615–22.
- Traba, J., P. Sastre, and M. B. Morales. 2013. "Factors Determining Species Richness and Composition of Steppe Bird

- Communities in Peninsular Spain: Grass-Steppe vs. Shrub-Steppe Bird Species.” In *Steppe Ecosystems: Biological Diversity, Management and Restoration*, edited by M. B. Morales and J. Traba, 47–72. New York, NY: NOVA Science Publishers.
- Upadhyay, P., S. K. Ghosh, and A. Kumar. 2013. “High Resolution Temporal Normalized Difference Vegetation Indices for Specific Crop Identification.” In *ISPRS - International Archives of the Photogrammetry, Remote Sensing and Spatial Information Sciences*, Vol. XL-1/W1, 351, 355.
- Vermeulen, C., P. Lejeune, J. Lisein, P. Sawadogo, and P. Bouché. 2013. “Unmanned Aerial Survey of Elephants.” *PLoS One* 8: e54700.
- Viña, A., A. A. Gitelson, A. L. Nguy-Robertson, and Y. Peng. 2011. “Comparison of Different Vegetation Indices for the Remote Assessment of Green Leaf Area Index of Crops.” *Remote Sensing of Environment* 115: 3468–78.
- Weiss, N., H. Zucchi, and A. Hochkirch. 2013. “The Effects of Grassland Management and Aspect on Orthoptera Diversity and Abundance: Site Conditions Are As Important as Management.” *Biodiversity and Conservation* 22: 2167–78.
- Weyer, J., J. Weinberger, and A. Hochkirch. 2012. “Mobility and Microhabitat Utilization in a Flightless Wetland Grasshopper, *Chorthippus Montanus* (Charpentier, 1825).” *Journal of Insect Conservation* 16: 379–90.
- Zurdo, J., J. Baonza, and J. Traba. 2021. “New Insights on Plant Communities and Flora of the Southern Paramos of the Iberian Range (Spain).” *Phytocoenologia* 50: 371–82.
- Zuur, A. F., E. N. Ieno, and A. A. Saveliev. 2017. *Beginner's Guide to Spatial, Temporal, and Spatial-Temporal Ecological Data Analysis with R-INLA*. Newburgh: Page Highland Statistics Ltd.

SUPPORTING INFORMATION

Additional supporting information can be found online in the Supporting Information section at the end of this article.

How to cite this article: Traba, J., J. Gómez-Catasús, A. Barrero, D. Bustillo-de la Rosa, J. Zurdo, I. Hervás, C. Pérez-Granados, E. L. García de la Morena, A. Santamaría, and M. Reverter. 2022. “Comparative Assessment of Satellite- and Drone-Based Vegetation Indices to Predict Arthropod Biomass in Shrub-Steppes.” *Ecological Applications* 32(8): e2707. <https://doi.org/10.1002/eap.2707>